ACS APPLIED BIO MATERIALS

www.acsabm.org Article

Three-Dimensional Tungsten Disulfide Raman Biosensor for Dopamine Detection

Noho Lee,[⊥] Myeong-Hwan Shin,[⊥] Eunho Lee, Seong-Hui Cho, Hyeonwoong Hwang, Kilwon Cho, Jong Kyu Kim,* and Sei Kwang Hahn*

Cite This: https://dx.doi.org/10.1021/acsabm.0c00876 Read Online

ACCESS | Metrics & More | Article Recommendations | Supporting Information

ABSTRACT: Two-dimensional (2D) transition metal dichalcogenides (TMDCs) are promising materials for detection of biomolecules due to their large surface-to-volume ratio. However, their poor response to the cellular environment hinders the realization of high-performance 2D TMDC sensors. Here, we present a hierarchical Raman scattering sensor consisting of the WS_2 directly grown on an array of three-dimensional (3D) WO_3 nanohelixes (NHs) by sulfurization. Both the adsorption of biomolecules and the proliferation of cells are significantly promoted for the 3D WS_2/WO_3 NH sensor compared to the control sensor with sulfurized WS_2 on 2D WO_3 film, leading to much enhanced sensitivity to dopamine. In addition, according to the *in vitro* test using PC12 cells, the 3D WS_2/WO_3 NH sensor shows a significant increase in hydrophobicity and Raman frequency shift, indicating that both the attachment of cells and the detection of biomolecules are improved.

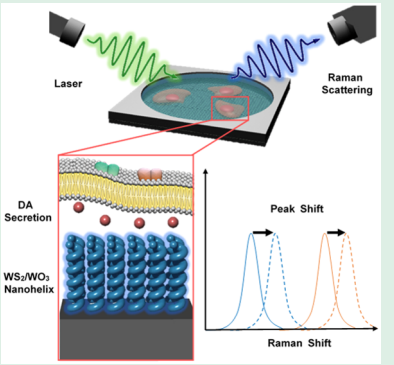

KEYWORDS: *tungsten disulfide, 3D nanostructure, Raman frequency shift, cytocompatibility, biomolecule detection*

1. INTRODUCTION

Dopamine (DA) is an important catecholamine neurotransmitter that plays a role in the functioning of the central nervous, hormonal, and cardiovascular systems. Abnormal DA levels could indicate diseases such as schizophrenia, Parkinson's disease, and HIV infection. Therefore, the detection of DA is important, but it is complicated due to low basal concentrations (0.01−1 μM) and the presence of interfering compounds in the extracellular fluid of the central nervous system.[1]

Recently, various analytical methods including electrochemical,[2] electrochemiluminescence,[3] fluorescence sensing,[4] and colormetry[5] were used for detecting DA. For example, a simple DA detection method based on fluorescence analysis was reported by Wei et al. (limit of detection (LOD) 0.3 μM).[4] Biosensing methods based on Raman scattering including surface-enhanced Raman scattering (SERS) and surface-enhanced resonance Raman scattering (SERRS) are widely used spectroscopic tools for detecting biomolecules because they are appropriate to obtain structural information about the systems of interest while performing sensitive biological or chemical detection.[6,7] Recently, Lu et al. have reported the silver nanocube-based ultrasensitive SERS detection of DA, which has a detection limit of 40 fM.[8] The spectra are sensitive to the doping state, enabling precise differentiation of the doping state by detecting small changes in the separation of first-order Raman modes.[9] However, traditional SERS using noble metal particles requires high cost and delicate procedures in fabrication for high performance.[10−12] Moreover, random distribution of plasmonic spots of SERS substrates significantly limits the reproducibility of SERS enhancement, impeding the practical application of SERS.[13−17]

Two-dimensional (2D) transition metal dichalcogenides (TMDCs) have attracted tremendous attention as emerging nanomaterials due to their earth-abundance, unique physical and chemical characteristics, and a wide variety of potential applications.[9,18,19] For example, TMDCs are very promising materials for biological systems due to their controllable photoelectrical properties, high stability, large surface area, and low levels of toxicity.[20] It was also reported that the adsorption of doping molecules on the surface of TMDCs can change the number of electrons extracted from the surface of TMDCs, inducing a Raman frequency shift that can be used for biomolecule sensor applications.[21] Based on such promising properties of TMDCs, lots of research has been actively carried out for enhancing the response and selectivity of biomolecular sensors. Besides, three-dimensional (3D) forms of 2D TMDCs have also been investigated due to their high specific surface

Received: July 15, 2020
Accepted: October 20, 2020

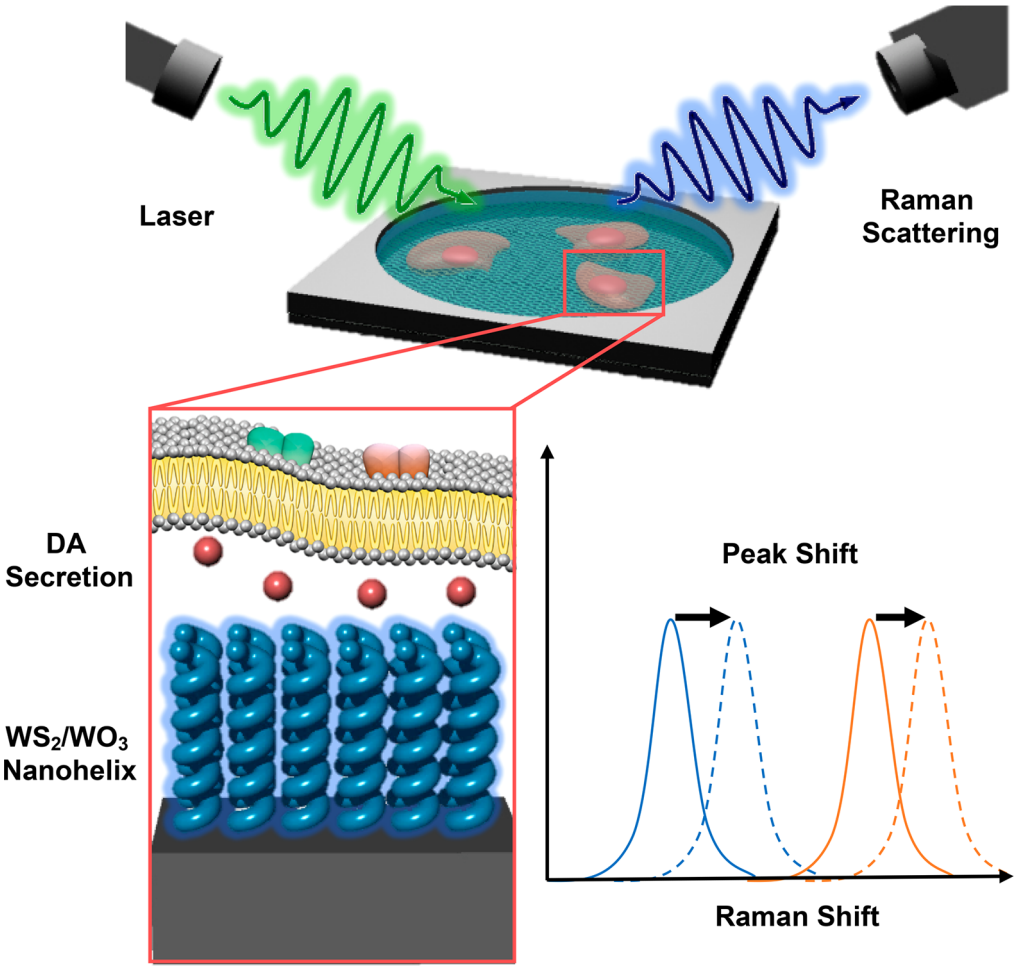

Figure 1. Schematic illustration of PC12 cell cultured WS_2/WO_3 NH Raman scattering biosensor with PDMS chamber for dopamine monitoring. The enlarged part shows the schematic structure of an array of WS_2/WO_3 NHs and DA secretion. DA induced peak-shift of Raman spectra is also schematically shown.

ratio and excellent biocompatibility and stability, thus, for biological, electronic, and catalytic applications.[22−26] Extension of the Raman biosensing platform into 3D nanostructures made of 2D TMDCs can enable promoted adsorption capacity, and thus sensing of biomolecules, while maintaining the advantages offered by TMDCs.[27]

In this study, we developed a hierarchical Raman scattering sensor consisting of 2D WS_2 directly grown on an array of 3D WO_3 nanohelixes (NHs) by a simple sulfurization process. The 3D WS_2/WO_3 NHs offers a large surface area and improved hydrophobicity, enabling a much enhanced affinity for protein−surface adsorption as well as a hydrophobic condensation effect.[28−31] This leads to not only improved adsorption of biomolecules but also promoted proliferation of cells, resulting in a large Raman frequency shift and, thus, high biomolecule-sensing performance.

2. EXPERIMENTAL SECTION

2.1. Materials. Dopamine hydrochloride (purity >98%, CAS 62-31-7), BSA (purity >98%, CAS 9048-46-8) and potassium chloride were purchased from Sigma-Aldrich (St. Louis, MO). PDMS (polydimethylsiloxane) and its curing agent was purchased from Dow Corning (Midland, MI). Biopsy punch was purchased from Miltex Inc., (Tethpage, NY). RPMI 1640, fetal bovine serum (FBS, CAS 9014-81-7), and horse serum were purchased from Invitrogen Co. (Calrsbad, CA). PC12 cells were obtained from Korean Cell Line Bank (Seoul, Korea). Dopamine ELISA kit was obtained from Abnova (Taipei, Taiwan).

2.2. Fabrication of Nanostructured WO_3. Tungsten (W) foils (1.5 cm × 2 cm in area, 0.05 mm in thickness, 99.95%, Nilaco, Japan) were used as a substrate for fabricating nanostructured WO_3. The array of WO_3 nanohelix (NH) was fabricated using an oblique angle deposition (OAD) method previously reported in the literature.[25,32] WO_3 powder (purity: 99.99%, Taewon Scientific Co., CAS 1314-35-8) contained in a graphite crucible was used as source. The oblique angle of the substrate was 80°, and the deposition was conducted at room temperature using an electron-beam evaporator. The thickness of the deposited WO_3 NH is ∼1 μm. Thin film (TF) WO_3 was deposited using the electron-beam evaporator with deposition rate of 2.0 Å/s. The thickness of deposited TF is ∼1 μm. Subsequently, the deposited WO_3 sample was annealed on muffle furnace (Daeheung Science, model DF-3.5) at 500 °C for 2 h as reported in our previous study.[25,32]

2.3. Sulfurization of the WO_3 NH. For direct growth of WS_2 from WO_3, annealed WO_3 was sulfurized in a 1-in.-diameter quartz tube furnace equipped in a chemical vapor deposition (CVD) system. The sulfur powder (purity > 99.5%, Sigma-Aldrich, CAS 7704-34-9) was used as precursor for the sulfurization. The sulfurization was conducted at 550 °C for 15 min with preannealed WO_3 samples loaded on the center of quartz tube and sulfur powder placed at the upstream side.[25,32]

2.4. Surface Characterization. Raman spectroscopy (Witech, Germany) employing a laser excitation of 532 nm was used initially to characterize the structure of the TF and nanohelix WS_2 sample.

https://dx.doi.org/10.1021/acsabm.0c00876
ACS Appl. Bio Mater. XXXX, XXX, XXX−XXX

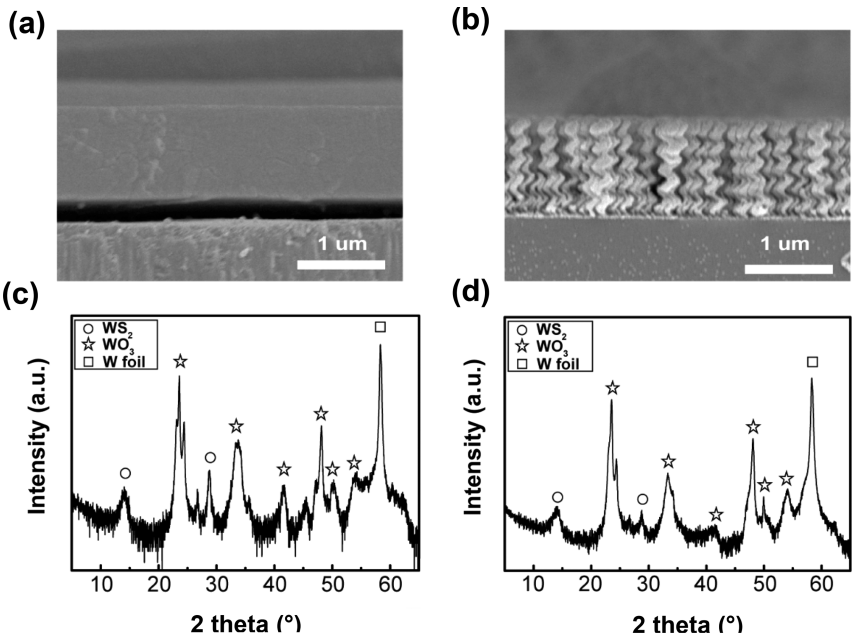

Figure 2. Microstructural characterization of the 2D thin film and 3D NH WS_2/WO_3 structures. (a, b) SEM images and (c, d) XRD profiles of the WS_2/WO_3 TF and NH on W foil, respectively.

Morphologies and microstructures were investigated by field-emission scanning electron microscopy (FE-SEM, Philips Electron Optics B.V., the Netherlands) and high resolution-transmission electron microscopy (HRTEM Jeol, Japan). The crystal structure of the samples was analyzed by X-ray diffraction (XRD) using an X-ray diffractometer (Rigaku Corporation, Japan) configured with a Cu Kα radiation source. High-performance X-ray photoelectron spectrometer (XPS Thermo Fisher Scientific, U.K) was used to obtain the bonding information and oxidation state of the samples.

Wettability was measured using contact angle measurement (Smartdrop, Femtofab). A 5 μL of DI water was dropped onto each specimen with an autopipette (Finnipette Novus, Thermo Scientific) at RT. The average contact angle was measured by the sessile drop method in three specimens for every groups.

2.5. PDMS Chamber Preparation. The chamber for protein adsorption and cell culture was prepared using a PDMS mold. PDMS solution and curing agent at a ratio of 1:10 (curing agent:base solution) were used for preparing PDMS mold with a method previously reported in the literature.[33] After the sterilization, the PDMS chamber was placed and fixed on the center of the WS_2/WO_3 surface.

2.6. BSA and Dopamine Adsorption Test. The protein and dopamine adsorption of each WS_2 was assessed using BSA and dopamine. Before the test, dopamine was conjugated with fluorescein isothiocyanate (FITC, Sigma-Aldrich, CAS 3326-32-7) using previously reported way for tracking the concentration. In brief, FITC-DA was synthesized through conjugation of the isothiocyanate reactive group (—N═C═S) of FITC to the primary amine group of DA. Conjugated dopamine at a concentration of 100 μg/mL was loaded on 2D TF or 3D NH WS_2/WO_3 for 1 h and the supernatant was harvested for loading content analysis. BSA at a concentration of 1 mg/mL was also loaded on each surface for 1 h and the protein concentration in the supernatant was analyzed by UV−vis spectroscopy.

2.7. Cell Proliferation Test and Confocal Imaging. PC12 cells were cultured on top of WS_2 devices to monitor the real-time secretion of dopamine from living cells. PC12 cells were cultured on the WS_2 devices for 24 h in the cell culture media (a mixture of RPMI, 10% horse serum, 1% antibiotic) and maintained at 37 °C in a humid atmosphere with 5% CO_2 air. Before the cell culture, each substrate was sterilized by immersing in 70% ethanol for 1 min after drying under UV lamp in the clean bench with continuous air flow for 30 min, the cells at a density of 6×10^3 mL^{-1} were cultured on each sample for further monitoring. The cultured cells were analyzed with cell counting kit-8 (CCK-8, Dojindo molecular technologies) solution for 1, 4, and 7 days after seeding.[34] Four samples were taken from each group to derive average value. The control group was the nontreated W foil.

To investigate the cellular morphology by confocal fluorescence microscopy, cells were fixed with 4% formaldehyde and PBS (Gibco) solution using the method previously reported in the literature.[34] Fluorescence images were observed using confocal microscopy (Leica TCS-SP5-MP-SMD, Leica Microsystems Wetzlar). The area of cell adhesion was measured using the ImageJ software (Sun Microsystems Inc.). To evaluate the average area per one cell, ten cells from each sample were investigated.

2.8. Raman Spectroscopy for Dopamine Detection. Raman spectra of DA bound substrate with concentrations ranging from 10 to 500 nM was recorded by confocal Raman spectroscopy (Ar-ion 633 nm excitation laser). The Raman spectrometer has been installed and leveled on a vibration-free desk in a darkroom. And also, the peak positions of Raman spectra were checked before and after the experiment with bare W foil sample. The spectra were recorded at 0.5 cm^{-1} intervals and the peak position extracted either by fit to a b-spline function after a calibration. Stimulation and sensing experiments were carried out after 1 h of replacing cell culture media with fresh ones. High potassium solution (the mixture of 40 mM NaCl, 105 mM KCl, 6 mM $CaCl_2$, 1 mM $MgCl_2$, and 10 mM HEPES) was prepared and introduced into the PDMS chamber. The two-dimensional Raman mapping (25 μm × 25 μm) on the surface was monitored during the high potassium stimulation.

2.9. Statistical Analysis. Statistical analysis was performed via *t* test using the software of SigmaPlot10.0 (Systat Software Inc. San Joce, CA). The value for $*p < 0.05$ and $**p < 0.01$ were considered statistically significant. Data are expressed as means ± standard deviation (SD) from several separate experiments. All experiments were done at least three times ($n \geq 3$).

3. RESULTS AND DISCUSSION

The overall scheme of a Raman scattering biosensor for DA detection is shown in Figure 1. For microsampling, an array of WO_3 NH was fabricated on W foil by using the OAD, followed by the growth of WS_2 by sulfurizing WO_3 NHs to form the

https://dx.doi.org/10.1021/acsabm.0c00876
ACS Appl. Bio Mater. XXXX, XXX, XXX−XXX

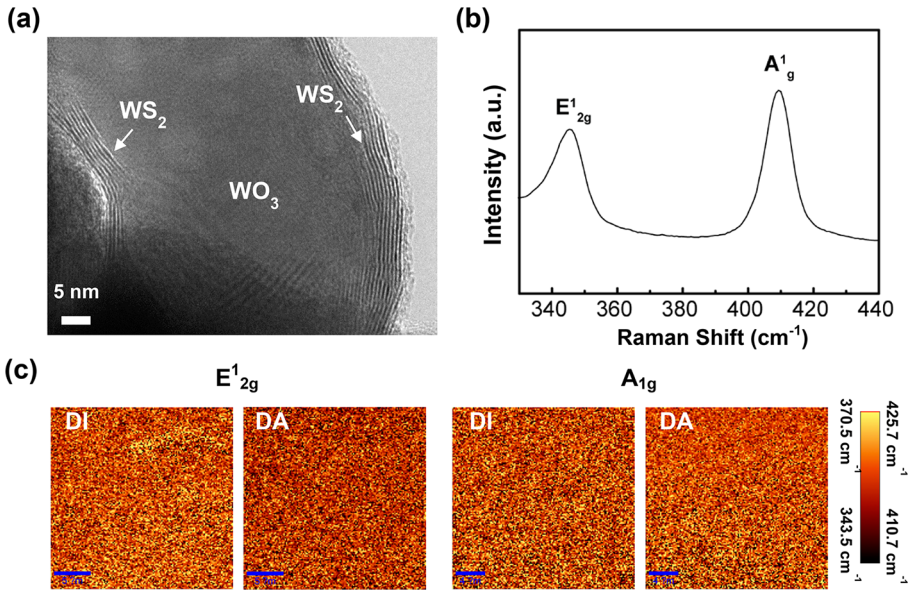

Figure 3. (a) TEM image of the WS_2/WO_3 NH showing WO_3 helical core and conformally formed WS_2 shell by sulfurization. (b) Raman spectra obtained from the WS_2 NH. (c) Raman maximum position mapping images of the WS_2 NH without (DI water) and with DA treatment (1 μM). Scale bar: 5 μm.

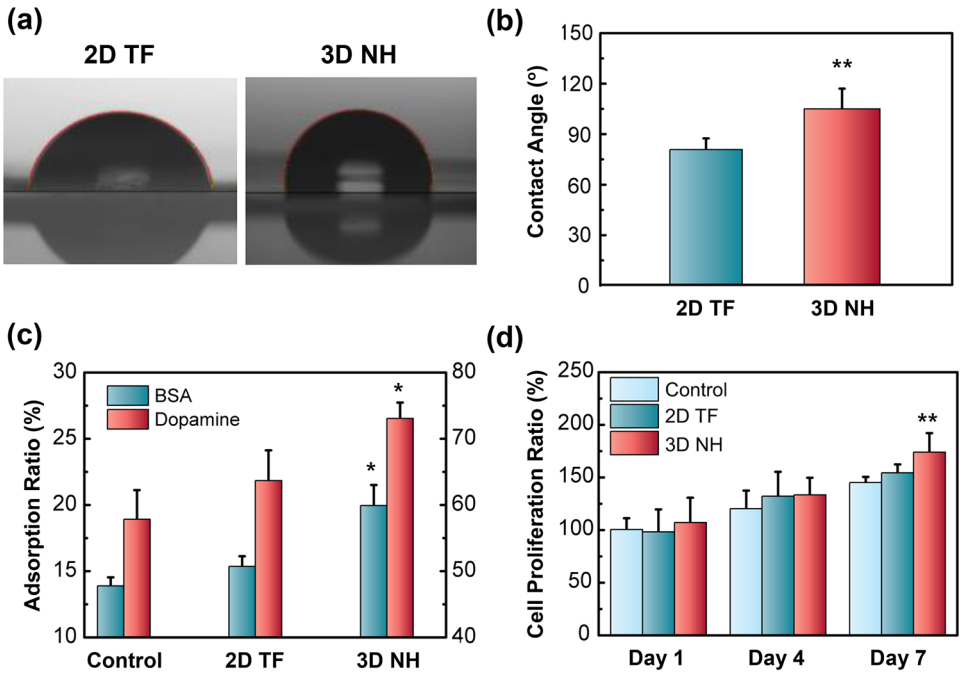

Figure 4. Characterizations of the WS_2/WO_3 NH compared to the WS_2/WO_3 TF. (a) Optical image of contact angle analysis, (b) quantification of contact angle analysis, (c) biomolecule adsorption test including BSA (left *y*-axis) and dopamine (right *y*-axis), and (d) PC12 cell proliferation test for 7 days on each substrate.

hierarchical WS_2/WO_3 NHs array as the detecting substrate (see experimental section for details). For protein adsorption and cell culture, PDMS mold with 5 mm hole (PDMS chamber) was placed and fixed on the center of W foil with the WS_2/WO_3 side of the substrate, so that the array of WS_2/WO_3 NH is exposed through the hole of PDMS mold. Subsequently, in PDMS chamber, the exposed WS_2/WO_3 NH was used for growing PC12 cells and detection of DA by attaching DA molecules, where the Raman frequency shift of WS_2 depending on the DA concentration was monitored.

To compare its characteristics with typical 2D TF structure, WS_2 was also directly grown on WO_3 TF on W foil by same sulfurization process. The microstructural properties of the 3D WS_2/WO_3 NH and the 2D TF structure were characterized as shown in Figure 2 (further denoted as 3D NH and 2D TF, respectively). Figure 2a and b are SEM images, showing clear difference in morphology between 3D NH and 2D TF. Especially, Figure 2b shows a well-defined array of NHs formed on the W foil with a thickness of 1 μm. The growth of WS_2 on the WO_3 NHs was also confirmed by XRD profiles shown in Figure 2c and d, with XRD peaks of WS_2 (JCPDS no.

https://dx.doi.org/10.1021/acsabm.0c00876
ACS Appl. Bio Mater. XXXX, XXX, XXX−XXX

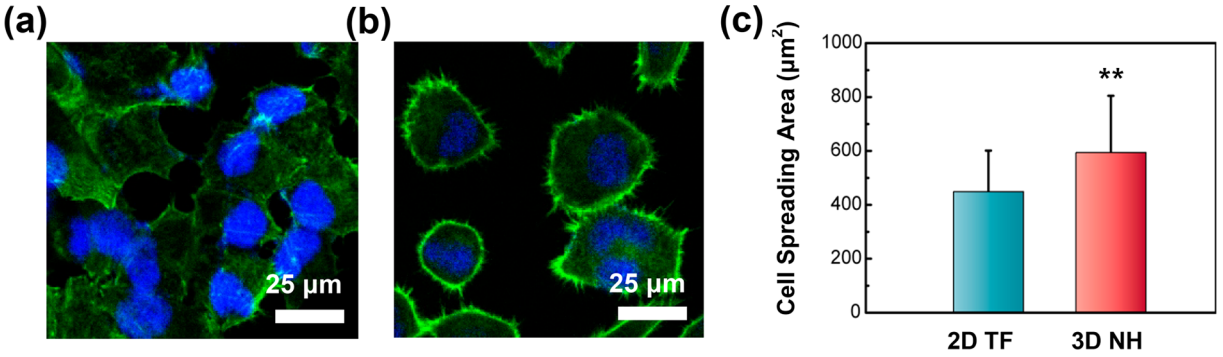

Figure 5. Fluorescence images of F-actin (pseudogreen) and nucleus (blue) stained cells after 3 days of PC12 cell culture on the 2D TF showing (a) aggregation of nucleus and round shape without stretched matrix and on the (b) 3D NH showing star-like shapes with apparent stretched matrix. (c) Measured average cell adhesion area on each substrate form the region of F-actin.

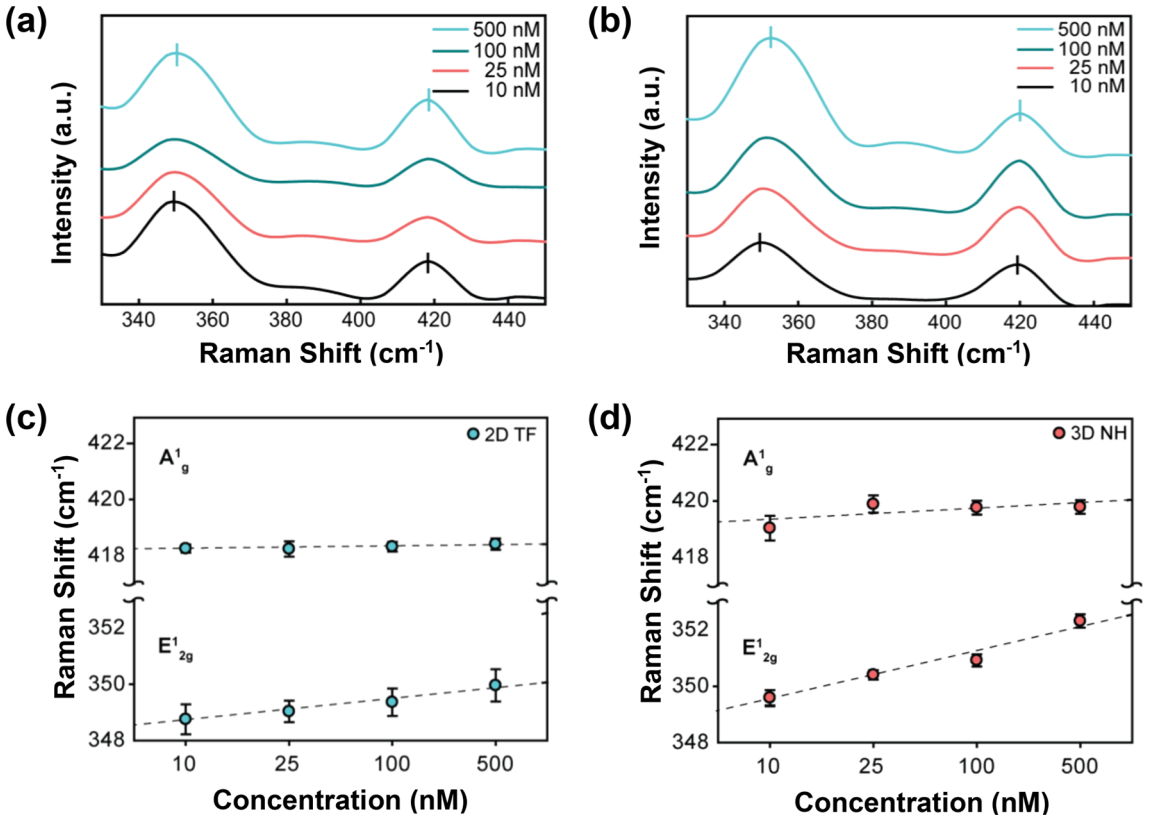

Figure 6. Raman spectra of WS_2 of (a) 2D TF and (b) 3D NH after the dopamine treatment with different concentrations. E^1_{2g} and A^1_g peaks position shifts of (c) 2D TF and (d) 3D NH upon doping with different concentrations.

08-0237) near 14° and those of WO_3 (JCPDS no. 43-1035) in both samples.

The microstructure of the WS_2/WO_3 NH was further analyzed by using TEM. As shown in Figure 3a, layered 2D WS_2 is formed on the surface of 3D WO_3 like a core−shell structure. The Raman spectrum obtained from the WS_2/WO_3 NH is shown in Figure 3b. E^1_{2g} and A^1_g represent characteristic peaks that arise from the in-plane and out-of-plane W—S vibration mode, which appears at 354 and 420 cm^{-1}, respectively. Figure 3c is the Raman mapping showing the maximum peak position of each peak near E^1_{2g} and A^1_g, respectively, with the DA concentration (0 for DI and 1 μM). Note that the Raman signal is distributed uniformly on the overall substrate indicating the uniform Raman sensing agility of our method (Figure 3c).

In addition, it was found that the surface of the 3D NH shows more hydrophobic character compared to that of the 2D TF. Hydrophobic surfaces can concentrate dissolved solution in aqueous droplets efficiently, known as the hydrophobic condensation effect and,[30,31] thus, can be used for active and effective Raman scattering substrates. To estimate the degree of hydrophobicity of the WS_2 depending on its nanostructure, contact angle measurement was performed without a specific surface treatment (Figure 4a).[35] The surface of the 3D NH showed higher contact angle than that of the 2D TF, as shown in Figure 4b (**$p < 0.01$, see the Experimental Section for details about statistical analysis). Since protein adsorption and cell activity are influenced by wettability, those properties were further analyzed, as shown in Figure 4c. A model protein, bovine serum albumin (BSA) at a concentration of 1 mg/mL

https://dx.doi.org/10.1021/acsabm.0c00876
ACS Appl. Bio Mater. XXXX, XXX, XXX−XXX

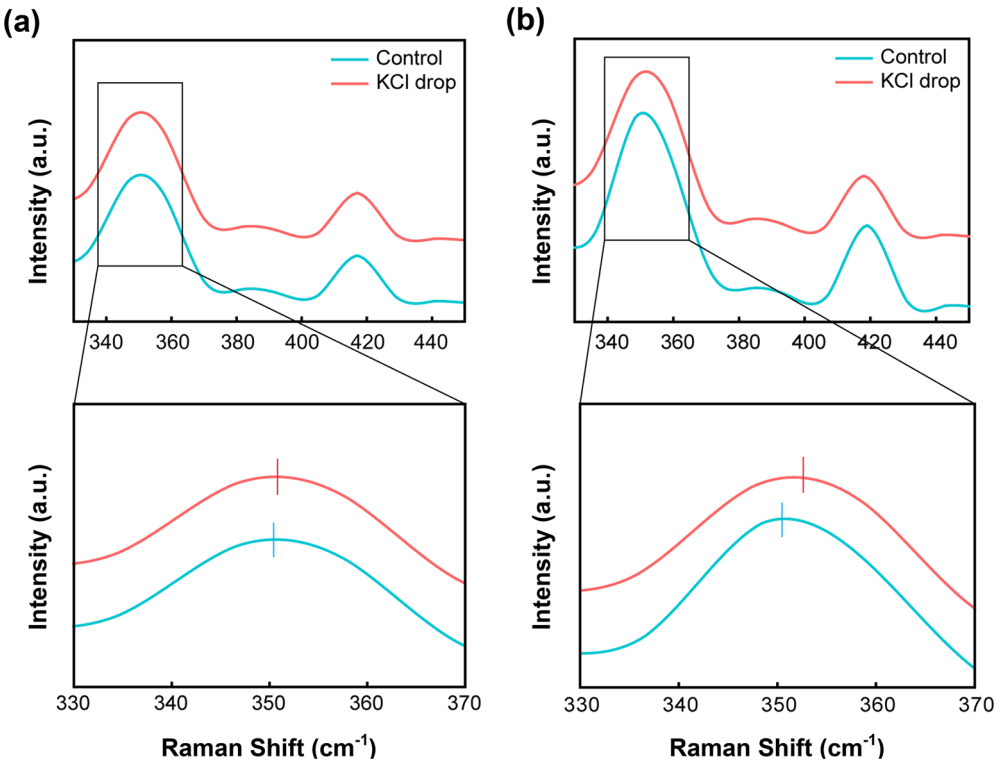

Figure 7. Raman shift of (a) the 2D TF and (b) the 3D NH biosensor to the secretion of DA from PC12 cells stimulated by high K^+ solution.

was loaded on each sample and the protein concentration in the supernatant was analyzed. After 1 h of the protein loading, 19.96% ± 1.56% of the protein could be loaded on the 3D NH which is higher than that of the 2D TF (15.36 ± 0.78%, $*p < 0.05$). Also, adsorption test of DA shows 63.7% and 73.1% for the 2D and the 3D structure, respectively ($*p < 0.05$). Higher adsorption rate of BSA and DA in the 3D NH is derived from more hydrophobic surface. Furthermore, cellular activities depending on the structure was assessed. Figure 4d shows the cell proliferation test of PC12 cells on the surface of each sample investigated after cell seeding for 4 and 7 days. The results show the proliferation ratio of the cells on the 3D NH was higher than that on the control and the 2D TF samples. The 3D NH can also affect the morphology of cell differentiation so that cells spread uniformly with a star-shape, which will be shown later. Taken together, the adsorption of protein can be enhanced through the increased hydrophobicity by the unique 3D nanostructure, and as a result, the cell proliferation was promoted.

As aforementioned, behavior of cells on each sample was also monitored. Confocal fluorescence microscope imaging of F-actin (phalloidin rhodamine; pseudo green) and nucleus (DAPI; blue) stained PC12 cells on each sample were shown in Figure 5a (2D TF) and b (3D NH). Cells on the 2D TF tends to aggregate to each other, whereas those on the 3D NH spread uniformly over the substrate with a star-shaped border morphology. The morphological difference is similar to previous reports showing positive effect to cells using nanotopography.[36] For example, the protein adsorption properties and cell activity can be enhanced by strong hydrophobic interaction occurring at the surface as shown in Figure 4. As a result, the hydrophobic nature of 3D nanostructured WS_2 allows cell to spread out widely during the cell proliferation.[37] In addition, the 3D NH shows the higher average cell adhesion area per one cell than the 2D TF ($**p < 0.01$) as shown in Figure 5c, indicating that the 3D NH structure enables a promoted cell growth over broad area. These results can be elucidated by the increased affinity of cell attachment caused by the surface roughness as well as enhanced protein adsorption ratio from its nanostructure as shown in Figure 4c.

After the cell proliferation test depending on the microstructure, we investigated its Raman sensing capability. Figure 6a and b show Raman spectra for the 2D and the 3D WS_2 with various DA doping concentrations. Blue shift of the Raman peaks was observed after doping to both samples, indicating the molecules cause the stiffening of vibrational modes. Figure 6c and d show quantitative peak position of both peaks. As the concentration of DA increased, the samples exhibited more Raman-frequency-shift, and which are more distinct in 3D NH than 2D TF sample. For the 3D NH sample, definite peak shift was shown in the range of 10−500 nM with a limit of detection (LOD) as low as 10 nM.

From Figure 6c and d, it is shown that the E^1_{2g} peak is blue-shifted as the concentration of DA was increased while the A^1_g peak is rarely unchanged. According to the previous reports, A^1_g mode frequency is sensitive to carrier doping, while the frequency of E^1_{2g} mode is more sensitive to strain.[38,39] In addition, it was shown that compressive strain can induce stiffening of E^1_{2g} mode. In this regards, it can be inferred that the adsorption of DA induces the compressive strain on the WS_2.[40,41] The difference in Raman frequency-shift between 2D TF and 3D NH can be explained by the different DA adsorption behavior due to differences in surface area and hydrophobicity of the 2D and 3D samples, as described above.

In addition to the detection ability, selective detection of DA is challenging due to potential interference with other substances in biological systems. In order to check selective

https://dx.doi.org/10.1021/acsabm.0c00876
ACS Appl. Bio Mater. XXXX, XXX, XXX−XXX

detection ability of the Raman biosensor, Raman sensing of DA was investigated in the environment where DA coexist with ascorbic acid (AA) or uric acid that usually coexists with DA in central nervous system. To evaluate the applicability and selectivity of our method, UA and AA were tested under the same conditions with the DA concentration of 10 nM and AA or UA concentration of 50 nM (Figure S1). The Raman frequency shift does not show an obvious change with these interfering substance even at the high concentration of 50 nM, indicating that, the Raman biosensor has an excellent selectivity for the detection of DA. The previously reported performance of DA sensor was listed in Table S1. Although our Raman biosensor shows comparably lower performance than other reports, the 3D WS_2 NH biosensor still has advantage in fast and facile detecting process. In addition, we believe that the detection capability as well as selectivity can be further improved by selection of materials, controlling the phase of the materials, and optimization of 3D nanostructure. From these results, the 3D nanostructured WS_2 shows the possibility of being used for DA sensing using the Raman frequency-shift with negligible interference with AA and UA.

In addition, we combined the 3D NH with the live neuroendocrine PC12 cells and detected the induction of dopamine secretion. PC12 cells were cultured directly on 3D NH without any treatment. When a K^+ solution was introduced into the recording PDMS chamber that depolarizes the cell membrane and induces Ca^{2+} influx through the voltage-gated calcium channels of the cell membrane, Raman frequency shift was monitored (Figure 7a and b). The Raman frequency shifts for the 3D NH is apparently larger than that of the 2D TF, which indicates that the 3D nanohelical structured WS_2/WO_3 biosensor can effectively detect very small amounts of biomolecule released by the cellular activity than 2D TF WS_2/WO_3. Taken together, the 3D WS_2 NH structure has very promising and beneficial properties for Raman scattering biomolecule sensor due to its much higher sensitivity, reproducibility, and cytocompatibility than the 2D structured WS_2. Furthermore, we believe that NH-based hierarchical structures can be a novel platform for not only a large variety of large-area biomedical and other industrial applications, but also chemical sensing and electrochemical energy harvesting applications.

4. CONCLUSIONS

We demonstrated a high performance nanostructured Raman scattering sensor based on hierarchical 2D WS_2 grown on an array of 3D WO_3 NHs. We observed that Raman frequency shift on the 3D nanohelical structured WS_2/WO_3 is much greater than that of the 2D thin film WS_2/WO_3 on the same concentration of DA doping, resulting the detection range of 10−500 nM with a LOD as low as 10 nM. Moreover, the cell proliferation test revealed that the promoted growth of uniform and star-shaped cell on 3D nanohelical structured WS_2/WO_3, which is attributed to an enhanced adsorption of biomolecules. As a result, it was shown that the 3D WS_2/WO_3 NH-based structure is very promising biosensing platform with high sensitivity, reproducibility. The enhanced cell proliferation and cytocompatibility of 3D WS_2/WO_3 further support the potential as biosensing platform through *in vitro* test. Furthermore, this research, we believe, provides the first comprehensive relationship between the adsorption behavior of biomolecules and the nanostructure of WS_2, as well as, key factors for solving limitation of previous 2D TMDCs sensor mostly based on film structure.

■ ASSOCIATED CONTENT

Supporting Information

The Supporting Information is available free of charge at https://pubs.acs.org/doi/10.1021/acsabm.0c00876.

Experimental data for dopamine selectivity and comparison table of previous studies on dopamine sensors (PDF)

■ AUTHOR INFORMATION

Corresponding Authors

Jong Kyu Kim − *Department of Materials Science and Engineering, Pohang University of Science and Technology (POSTECH), Pohang, Gyeongbuk 37673, Korea;* orcid.org/0000-0003-1643-384X; Phone: +82-54-279-2149; Email: kimjk@postech.ac.kr; Fax: +82-54-279-5837

Sei Kwang Hahn − *Department of Materials Science and Engineering, Pohang University of Science and Technology (POSTECH), Pohang, Gyeongbuk 37673, Korea; PHI BIOMED Co., Seoul 06612, Korea;* orcid.org/0000-0002-7718-6259; Phone: +82 54 279 2159; Email: skhanb@postech.ac.kr; Fax: +82-54-279-2399

Authors

Noho Lee − *Department of Materials Science and Engineering, Pohang University of Science and Technology (POSTECH), Pohang, Gyeongbuk 37673, Korea;* orcid.org/0000-0002-4339-8974

Myeong-Hwan Shin − *Department of Materials Science and Engineering, Pohang University of Science and Technology (POSTECH), Pohang, Gyeongbuk 37673, Korea*

Eunho Lee − *Department of Chemical Engineering, Pohang University of Science and Technology (POSTECH), Pohang, Gyeongbuk 37673, Korea*

Seong-Hui Cho − *Department of Materials Science and Engineering, Pohang University of Science and Technology (POSTECH), Pohang, Gyeongbuk 37673, Korea*

Hyeonwoong Hwang − *Department of Materials Science and Engineering, Pohang University of Science and Technology (POSTECH), Pohang, Gyeongbuk 37673, Korea*

Kilwon Cho − *Department of Chemical Engineering, Pohang University of Science and Technology (POSTECH), Pohang, Gyeongbuk 37673, Korea;* orcid.org/0000-0003-0321-3629

Complete contact information is available at: https://pubs.acs.org/10.1021/acsabm.0c00876

Author Contributions

⊥These authors contributed equally.

Notes

The authors declare no competing financial interest.

■ ACKNOWLEDGMENTS

This research was supported by the National Research Foundation of Korea (NRF) grant funded by the Korea government (MSIT) (No. 2020R1A2C3014070). Also, this work was supported by Global Frontier Project (CASE 2015M3A6A5072945), Global Ph.D. Fellowship Program (2015H1A2A1034046 and 2017H1A2A1042400), and Technology Development Program to Hydrogen Energy (NRF

https://dx.doi.org/10.1021/acsabm.0c00876
ACS Appl. Bio Mater. XXXX, XXX, XXX−XXX

2019M3E6A1064521) of the National Research Foundation (NRF) funded by the Ministry of Science, ICT & Future Planning, Korea.

REFERENCES

(1) Kaya, M.; Volkan, M. New Approach for the Surface Enhanced Resonance Raman Scattering (SERRS) Detection of Dopamine at Picomolar (PM) Levels in the Presence of Ascorbic Acid. *Anal. Chem.* **2012**, *84* (18), 7729−7735.
(2) Yang, C.; Hu, K.; Wang, D.; Zubi, Y.; Lee, S. T.; Puthongkham, P.; Mirkin, M. V.; Venton, B. J. Cavity Carbon-Nanopipette Electrodes for Dopamine Detection. *Anal. Chem.* **2019**, *91* (7), 4618−4624.
(3) Wu, B.; Miao, C.; Yu, L.; Wang, Z.; Huang, C.; Jia, N. Sensitive Electrochemiluminescence Sensor Based on Ordered Mesoporous Carbon Composite Film for Dopamine. *Sens. Actuators, B* **2014**, *195*, 22−27.
(4) Wei, X.; Zhang, Z.; Wang, Z. A Simple Dopamine Detection Method Based on Fluorescence Analysis and Dopamine Polymerization. *Microchem. J.* **2019**, *145*, 55−58.
(5) Kong, B.; Zhu, A.; Luo, Y.; Tian, Y.; Yu, Y.; Shi, G. Sensitive and Selective Colorimetric Visualization of Cerebral Dopamine Based on Double Molecular Recognition. *Angew. Chem., Int. Ed.* **2011**, *50* (8), 1837−1840.
(6) Graniel, O.; Iatsunskyi, I.; Coy, E.; Humbert, C.; Barbillon, G.; Michel, T.; Maurin, D.; Balme, S.; Miele, P.; Bechelany, M. Au-Covered Hollow Urchin-like ZnO Nanostructures for Surface-Enhanced Raman Scattering Sensing. *J. Mater. Chem. C* **2019**, *7* (47), 15066−15073.
(7) Wang, Y.; Yan, B.; Chen, L. SERS Tags: Novel Optical Nanoprobes for Bioanalysis. *Chem. Rev.* **2013**, *113* (3), 1391−1428.
(8) Lu, D.; Fan, M.; Cai, R.; Huang, Z.; You, R.; Huang, L.; Feng, S.; Lu, Y. Silver Nanocube Coupling with a Nanoporous Silver Film for Dual-Molecule Recognition Based Ultrasensitive SERS Detection of Dopamine. *Analyst* **2020**, *145* (8), 3009−3016.
(9) Mitioglu, A. A.; Plochocka, P.; Deligeorgis, G.; Anghel, S.; Kulyuk, L.; Maude, D. K. Second-Order Resonant Raman Scattering in Single-Layer Tungsten Disulfide WS 2. *Phys. Rev. B: Condens. Matter Mater. Phys.* **2014**, *89* (24), 245442.
(10) Hahm, E.; Cha, M. G.; Kang, E. J.; Pham, X. H.; Lee, S. H.; Kim, H. M.; Kim, D. E.; Lee, Y. S.; Jeong, D. H.; Jun, B. H. Multilayer Ag-Embedded Silica Nanostructure as a Surface-Enhanced Raman Scattering-Based Chemical Sensor with Dual-Function Internal Standards. *ACS Appl. Mater. Interfaces* **2018**, *10* (47), 40748−40755.
(11) Mei, R.; Wang, Y.; Liu, W.; Chen, L. Lipid Bilayer-Enabled Synthesis of Waxberry-like Core-Fluidic Satellite Nanoparticles: Toward Ultrasensitive Surface-Enhanced Raman Scattering Tags for Bioimaging. *ACS Appl. Mater. Interfaces* **2018**, *10* (28), 23605−23616.
(12) Han, Y.; Wu, S. R.; Tian, X. D.; Zhang, Y. Optimizing the Sers Performance of 3d Substrates through Tunable 3d Plasmonic Coupling toward Label-Free Liver Cancer Cell Classification. *ACS Appl. Mater. Interfaces* **2020**, *12* (26), 28965−28974.
(13) Tan, Y.; Zang, X.; Gu, J.; Liu, D.; Zhu, S.; Su, H.; Feng, C.; Liu, Q.; Lau, W. M.; Moon, W. J.; et al. Morphological Effects on Surface-Enhanced Raman Scattering from Silver Butterfly Wing Scales Synthesized via Photoreduction. *Langmuir* **2011**, *27* (19), 11742−11746.
(14) Cong, S.; Yuan, Y.; Chen, Z.; Hou, J.; Yang, M.; Su, Y.; Zhang, Y.; Li, L.; Li, Q.; Geng, F.; Zhao, Z. Noble Metal-Comparable SERS Enhancement from Semiconducting Metal Oxides by Making Oxygen Vacancies. *Nat. Commun.* **2015**, *6*, 1−7.
(15) Mei, R.; Wang, Y.; Yu, Q.; Yin, Y.; Zhao, R.; Chen, L. Gold Nanorod Array-Bridged Internal-Standard SERS Tags: From Ultrasensitivity to Multifunctionality. *ACS Appl. Mater. Interfaces* **2020**, *12* (2), 2059−2066.
(16) Jeong, S.; Kim, M. W.; Jo, Y. R.; Kim, N. Y.; Kang, D.; Lee, S. Y.; Yim, S. Y.; Kim, B. J.; Kim, J. H. Hollow Porous Gold Nanoshells with Controlled Nanojunctions for Highly Tunable Plasmon Resonances and Intense Field Enhancements for Surface-Enhanced Raman Scattering. *ACS Appl. Mater. Interfaces* **2019**, *11* (47), 44458−44465.
(17) Gomes, P. D. C.; Rickard, J. J. S.; Goldberg Oppenheimer, P. Electrofluidynamic Patterning of Tailorable Nanostructured Substrates for Surface-Enhanced Raman Scattering. *ACS Appl. Nano Mater.* **2020**, *3* (7), 6774−6784.
(18) Kurapati, R.; Kostarelos, K.; Prato, M.; Bianco, A. Biomedical Uses for 2D Materials Beyond Graphene: Current Advances and Challenges Ahead. *Adv. Mater.* **2016**, *28* (29), 6052−6074.
(19) Agrawal, A. V.; Kumar, R.; Venkatesan, S.; Zakhidov, A.; Zhu, Z.; Bao, J.; Kumar, M.; Kumar, M. Fast Detection and Low Power Hydrogen Sensor Using Edge-Oriented Vertically Aligned 3-D Network of MoS_2 Flakes at Room Temperature. *Appl. Phys. Lett.* **2017**, *111* (9), No. 093102.
(20) Ping, J.; Fan, Z.; Sindoro, M.; Ying, Y.; Zhang, H. Recent Advances in Sensing Applications of Two-Dimensional Transition Metal Dichalcogenide Nanosheets and Their Composites. *Adv. Funct. Mater.* **2017**, *27*, 1605817.
(21) Ko, K. Y.; Song, J. G.; Kim, Y.; Choi, T.; Shin, S.; Lee, C. W.; Lee, K.; Koo, J.; Lee, H.; Kim, J.; et al. Improvement of Gas-Sensing Performance of Large-Area Tungsten Disulfide Nanosheets by Surface Functionalization. *ACS Nano* **2016**, *10* (10), 9287−9296.
(22) Feng, X.; Zhang, Y.; Zhou, J.; Li, Y.; Chen, S.; Zhang, L.; Ma, Y.; Wang, L.; Yan, X. Three-Dimensional Nitrogen-Doped Graphene as an Ultrasensitive Electrochemical Sensor for the Detection of Dopamine. *Nanoscale* **2015**, *7* (6), 2427.
(23) Li, N.; Zhang, Q.; Gao, S.; Song, Q.; Huang, R.; Wang, L.; Liu, L.; Dai, J.; Tang, M.; Cheng, G. Three-Dimensional Graphene Foam as a Biocompatible and Conductive Scaffold for Neural Stem Cells. *Sci. Rep.* **2013**, *3*, 1604.
(24) Zhang, L.; Zhang, F.; Yang, X.; Long, G.; Wu, Y.; Zhang, T.; Leng, K.; Huang, Y.; Ma, Y.; Yu, A.; Chen, Y.; et al. Porous 3D Graphene-Based Bulk Materials with Exceptional High Surface Area and Excellent Conductivity for Supercapacitors. *Sci. Rep.* **2013**, *3*, 1408.
(25) Lee, N.; Choi, I. Y.; Doh, K. Y.; Kim, J.; Sim, H.; Lee, D.; Choi, S. Y.; Kim, J. K. Enhanced Catalytic Activity of Edge-Exposed 1T Phase WS2 Grown Directly on a WO3 Nanohelical Array for Water Splitting. *J. Mater. Chem. A* **2019**, *7* (46), 26378−26384.
(26) Zheng, B.; Chen, Y.; Qi, F.; Wang, X.; Zhang, W.; Li, Y.; Li, X. 3D-Hierarchical $MoSe_2$ Nanoarchitecture as a Highly Efficient Electrocatalyst for Hydrogen Evolution. *2D Mater.* **2017**, *4* (2), No. 025092.
(27) Ko, H.; Chang, S.; Tsukruk, V. V. Porous Substrates for Label-Free Molecular Level Detection of Nonresonant Organic Molecules. *ACS Nano* **2009**, *3* (1), 181−188.
(28) Zhang, H.; Zhou, F.; Liu, M.; Liu, D.; Men, D.; Cai, W.; Duan, G.; Li, Y. Spherical Nanoparticle Arrays with Tunable Nanogaps and Their Hydrophobicity Enhanced Rapid SERS Detection by Localized Concentration of Droplet Evaporation. *Adv. Mater. Interfaces* **2015**, *2* (9), 1500031.
(29) Lu, L. Q.; Zheng, Y.; Qu, W. G.; Yu, H. Q.; Xu, A. W. Hydrophobic Teflon Films as Concentrators for Single-Molecule SERS Detection. *J. Mater. Chem.* **2012**, *22* (39), 20986−20990.
(30) Li, Z.; Zhu, K.; Zhao, Q.; Meng, A. The Enhanced SERS Effect of Ag/ZnO Nanoparticles through Surface Hydrophobic Modification. *Appl. Surf. Sci.* **2016**, *377*, 23−29.
(31) Niu, D.; Tang, G. H. The Effect of Surface Wettability on Water Vapor Condensation in Nanoscale. *Sci. Rep.* **2016**, *6*, 19192.
(32) Lee, N.; Kwak, J.; Kwak, J. H.; Jung, S. M.; Kim, J.; Giri, A.; Thiyagarajan, K.; Kim, Y. T.; Jung, S.; Kim, J. K.; et al. Microwave-Assisted Evolution of WO3and WS2/WO3hierarchical Nanotrees. *J. Mater. Chem. A* **2020**, *8* (19), 9654−9660.
(33) Jung, H. S.; Kim, H. H.; Shin, M. H.; Kim, S.; Kim, K. S.; Cho, K.; Hahn, S. K. Electroceutical Residue-Free Graphene Device for Dopamine Monitoring and Neural Stimulation. *ACS Biomater. Sci. Eng.* **2019**, *5* (4), 2013−2020.

https://dx.doi.org/10.1021/acsabm.0c00876
ACS Appl. Bio Mater. XXXX, XXX, XXX−XXX

(34) Shin, M. H.; Baek, S. M.; Polyakov, A. V.; Semenova, I. P.; Valiev, R. Z.; Hwang, W. B.; Hahn, S. K.; Kim, H. S. Molybdenum Disulfide Surface Modification of Ultrafine-Grained Titanium for Enhanced Cellular Growth and Antibacterial Effect. *Sci. Rep.* **2018**, *8* (1), 9907.
(35) Lee, J.; Dak, P.; Lee, Y.; Park, H.; Choi, W.; Alam, M. A.; Kim, S. Two-Dimensional Layered MoS_2 Biosensors Enable Highly Sensitive Detection of Biomolecules. *Sci. Rep.* **2015**, *4*, 1−7.
(36) Chen, Z.; Visalakshan, R. M.; Guo, J.; Wei, F.; Zhang, L.; Chen, L.; Lin, Z.; Vasilev, K.; Xiao, Y. Plasma Deposited Poly-Oxazoline Nanotextured Surfaces Dictate Osteoimmunomodulation towards Ameliorative Osteogenesis. *Acta Biomater.* **2019**, *96*, 568−581.
(37) Visalakshan, R. M.; Macgregor, M. N.; Sasidharan, S.; Ghazaryan, A.; Mierczynska-Vasilev, A. M.; Morsbach, S.; Mailänder, V.; Landfester, K.; Hayball, J. D.; Vasilev, K. Biomaterial Surface Hydrophobicity-Mediated Serum Protein Adsorption and Immune Responses. *ACS Appl. Mater. Interfaces* **2019**, *11* (31), 27615−27623.
(38) Iqbal, M. W.; Shahzad, K.; Akbar, R.; Hussain, G. A Review on Raman Finger Prints of Doping and Strain Effect in TMDCs. *Microelectron. Eng.* **2020**, *219*, 111152.
(39) Li, Y.; Xu, C. Y.; Hu, P.; Zhen, L. Carrier Control of MoS2 Nanoflakes by Functional Self-Assembled Monolayers. *ACS Nano* **2013**, *7* (9), 7795−7804.
(40) Singh, A.; Sharma, G.; Singh, B. P.; Vasa, P. Charge-Induced Lattice Compression in Monolayer MoS2. *J. Phys. Chem. C* **2019**, *123* (29), 17943−17950.
(41) Su, W.; Dou, H.; Huo, D.; Dai, N.; Yang, L. Enhancing Photoluminescence of Trion in Single-Layer MoS2 Using p-Type Aromatic Molecules. *Chem. Phys. Lett.* **2015**, *635*, 40−44.

https://dx.doi.org/10.1021/acsabm.0c00876
ACS Appl. Bio Mater. XXXX, XXX, XXX−XXX